frontiers | Frontiers in Earth Science

ORIGINAL RESEARCH
published: 05 May 2022
doi: 10.3389/feart.2022.865761

Timing of Sedimentary Evolution and Transgressions in the Bohai Sea During the Last ~200 ka: Constraints from Luminescence Dating of a Core from the Yellow River Delta

Xin Zhang[1,2], *Jian Liu*[1,2]*, *Yixuan Wang*[3]*, *Tianyuan Chen*[3], *Mahmoud Abbas*[4†] and *Shengling Qian*[5]

[1]Qingdao Institute of Marine Geology, Qingdao, China, [2]Laboratory for Marine Geology, Qingdao National Laboratory for Marine Science and Technology, Qingdao, China, [3]Key Laboratory of Comprehensive and Highly Efficient Utilization of Salt Lake Resources, Qinghai Institute of Salt Lakes, Chinese Academy of Sciences, Xining, China, [4]Institute of Marine Sciences, Guangdong Provincial Key Laboratory of Marine Disaster Prediction and Protection, Shantou University, Shantou, China, [5]East-China Metallurgical Institute of Geology and Exploration, Hefei, China

The southwestern coast of the Bohai Sea is a favorable area to study land-sea interactions and palaeoenvironmental changes. The Bohai Sea hosts vast volumes of sediment discharged from rivers of mainland China and has undergone large-scale sea-level fluctuations during the Quaternary. Three transgressions have been previously determined for the Bohai Sea since the late Pleistocene. However, the timings of the two earlier transgressions are still unclear. Here we present chronological, micropalaeontological, and sedimentological data for an 80-m-long sediment core recovered from the modern Yellow River delta. The changes in grain size and foraminiferal assemblages suggest the occurrence of three marine sedimentary units, M-3, M-2, and M-1, that represent transgressions of the Bohai Sea. We applied optically stimulated luminescence dating using both quartz and feldspar minerals on 15 samples obtained from core YRD-1401 and eight radiocarbon ages using fragments of microfossils shells and organic carbon. Our quartz optically stimulated luminescence ages for M-2 (*ca*. 60 ka), are consistent with K-feldspar post-infrared stimulated luminescence ages, suggesting that M-2 on the southwestern coast of the Bohai Sea was deposited during early MIS 3. The sea level of the Bohai Sea during early MIS 3 is estimated to have ranged from 26.8 to 19.9 m below the present sea level. Luminescence ages and foraminiferal assemblages indicate that M-3 was likely formed during MIS 5 and a tidal-river environment prevailed on the southwestern coast of the Bohai Sea during MIS 6 or earlier.

Keywords: Bohai Sea, pleistocene, transgression, MIS 3, sea-level change, luminescence dating, sedimentary environment

OPEN ACCESS

Edited by:
Daidu Fan,
Tongji University, China

Reviewed by:
Zhengquan Yao,
Ministry of Natural Resources, China
Yuan-Pin Chang,
National Sun Yat-sen University, Taiwan

***Correspondence:**
Jian Liu
liujian0550@vip.sina.com
Yixuan Wang
yixuanwang@isl.ac.cn

†ORCID ID:
Mahmoud Abbas
orcid.org/0000-0003-4447-2280

Specialty section:
This article was submitted to Quaternary Science, Geomorphology and Paleoenvironment, a section of the journal Frontiers in Earth Science

Received: *30 January 2022*
Accepted: *07 April 2022*
Published: *05 May 2022*

Citation:
Zhang X, Liu J, Wang Y, Chen T, Abbas M and Qian S (2022) Timing of Sedimentary Evolution and Transgressions in the Bohai Sea During the Last ~200 ka: Constraints from Luminescence Dating of a Core from the Yellow River Delta. Front. Earth Sci. 10:865761. doi: 10.3389/feart.2022.865761

INTRODUCTION

Sea-level change has fluctuated in response to climatic oscillations during the Quaternary period, ranging from ~10 m above to ~130 m below the present level during climatic cycles (e.g., Chappell et al., 1996; Lambeck and Chappell, 2001). The coastal areas of eastern China act as a pathway to transport terrestrial sediments to the ocean. Sea-level fluctuations caused coastal zones to undergo strong environmental variations, as indicated by the alternation of marine and fluvial environments (e.g., Shi et al., 2016; Liu et al., 2018; Ronchi et al., 2018). Consequently, coastal areas contain records of past environments and are also vulnerable environments against a background of continuing global warming, being extremely sensitive to even minor sea-level changes. In addition, coastal areas are a focus, of intense scientific and social attention because of the high population density and economic influence of these areas (Hinkel et al., 2014).

Studies of borehole cores drilled in marginal seas off eastern China have reported the widespread existence of three marine sedimentary units, namely, M-3, M-2, and M-1 (in ascending order) during the late Pleistocene and Holocene, corresponding to three major transgressions (Yi et al., 2012; Shang et al., 2018; Xu et al., 2018; Li et al., 2019; Dai et al., 2021). Radiocarbon dates have confirmed the formation of M-1 during the Holocene (e.g., Zhang et al., 2016; Li et al., 2019); however, the ages of M-2 and M-3 in the coastal to shelf areas of eastern China are uncertain. Early ^{14}C dating results for M-2 ranged from 45 to 30 ka (i.e., middle to late Marine Isotope Stage 3 (MIS 3, *ca.* 60–25 ka; Lisá et al., 2018)) (e.g., Zhao et al., 1978; Shang et al., 2018), but these ages are near the older limit of radiocarbon dating, and hence should be re-evaluated (Pigati et al., 2007; Manaa et al., 2016; Miller and Andrews, 2019). In addition, an incomplete stratigraphic record may compromise the reliability of magnetostratigraphy (Liu et al., 2014). Consequently, it seems doubtful that M-2 and M-3 were deposited during the MIS 3 and MIS 5 (*ca.* 128–73 ka; Lisiecki and Raymo, 2005), respectively, as inferred from sediments dated using radiocarbon chronology and/or geomagnetic excursion events.

Radiocarbon ages of pre-Holocene marine sediments in Hong Kong have proven to be much younger than U-series dates of molluscs (Yim et al., 1990), which indicates the limited ability of radiocarbon dating to constrain the timing of M-2 and M-3. Therefore, it is essential to conduct a comprehensive and systematic chronological investigation to provide a better understanding of the sedimentary evolution of coastal to shelf areas of eastern China using a combination of radiocarbon and optically stimulated luminescence (OSL) ages (e.g., Jacobs, 2008; Reimann et al., 2010; Neudorf et al., 2015; Nian et al., 2021). In contrast to ^{14}C dating, OSL is more suitable for dating sedimentary events back to 100 to 25 ka or older (e.g., Olley et al., 1998; Pawley et al., 2010; Murray et al., 2021). OSL ages have challenged the widely held view that M-2 and M-3 formed during MIS 3 and MIS 5, respectively. OSL dating has constrained M-2 to MIS 5 and M-3 to MIS 7 (Chen et al., 2012; Gao et al., 2021). It was thus anticipated that other studies would report similar age results for M-2 using OSL. However, OSL dates of a recent study demonstrated that M-2 in Liaodong Bay was deposited during MIS 3 (Li et al., 2019). Hence, a consensus regarding the ages of M-2 and M-3 is still lacking.

Precise ages of these marine sedimentary units are key to solving the unclear transgression chronology. Luminescence dating has been widely applied to coastal and marine sediments and has proved successful in exploring the evolution of Quaternary sedimentary environments (Murray and Wintle, 2000; Jacobs, 2008; Lamothe, 2016). However, the fast components of the quartz OSL signals have been shown to be saturated at a relatively low dose (*ca.* 200 Gy), leading to age underestimations (e.g., Buylaert et al., 2007; Murray et al., 2007; Lai, 2010; Timar et al., 2010; Lowick and Preusser, 2011). The infrared stimulated luminescence (IRSL) signal outperforms that of quartz OSL in terms of saturation dose levels (Li et al., 2007; Li et al., 2014), and can provide better constraints on older samples (300–200 ka). Therefore, it is necessary to combine quartz OSL with feldspar IRSL dating to constrain the timings of stratigraphic sequences for comparison purposes.

With the advent of micropalaeontology, benthic foraminifera has been increasingly used to identify distinct environments and reveal the palaeoenvironmental evolution of regions (e.g., De Rijk et al., 1999; Frontalini and Coccioni, 2008; Anbuselvan and Senthil, 2018). Benthic foraminifera lives in marine and transitional environments and show a clear zonation with respect to parameters such as salinity and water depth, indicating their response to environmental change (Romano et al., 2018). Moreover, rivers may develop in coastal areas and incise the underlying strata during periods of low sea level, represented by multiple unconformities in the sedimentary record (Fagherazzi et al., 2008). In summary, the absence of benthic foraminiferal data and/or incompleteness of the sedimentary record may obstruct to clear discrimination of M-2 and M-3 sedimentary units of coastal eastern China. Given the complexity of the stratigraphic sequence and chronological framework for the late Quaternary, further studies of the sedimentary record in and around the Bohai Sea are needed.

In this study, an 81.0-m-long core (YRD-1401) was recovered from the modern Yellow River delta on the southwestern coast of the Bohai Sea. Quartz OSL, K-feldspar post-infrared stimulated luminescence (pIRIR), and accelerator mass spectrometry (AMS) ^{14}C dating were combined to better constrain the timings of transgressions in the Bohai Sea. We aim to establish a reliable chronological framework and clarify the sedimentary evolution of the western Bohai Sea during the last ~200 ka. The results yield insights into transgressive events that have occurred since 200 ka, terrestrial–marine interaction, and the sedimentary history of the Bohai Sea.

GEOLOGICAL SETTING

The Bohai Sea is a shallow and semi-enclosed sea of eastern China, covering an area of ~7.8×10^4 km^2, and connects to the North Yellow Sea *via* the Bohai Strait (**Figure 1**). The average slope and water depths are 0.0078 and 18 m, respectively (Qin

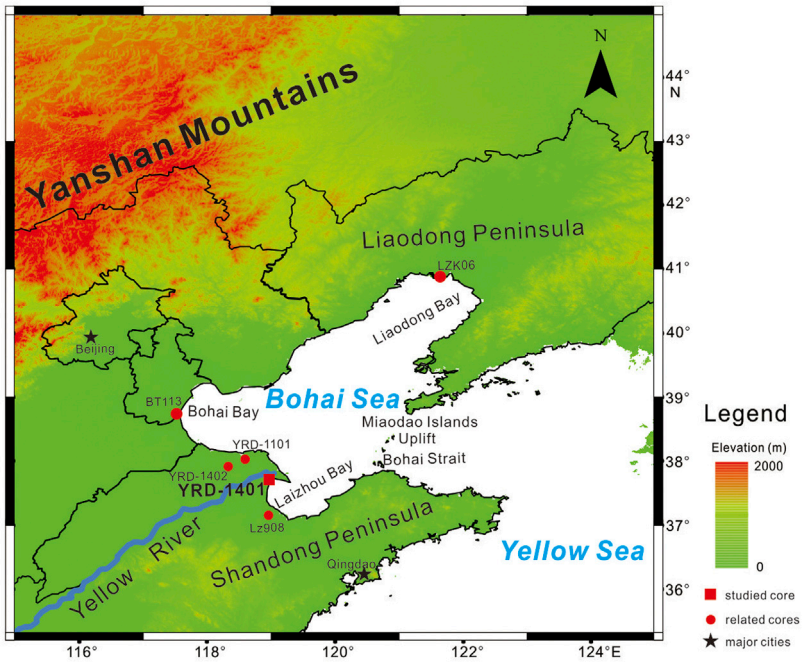

FIGURE 1 | Elevation map showing the study area and sediment cores. Core YRD-1401 is marked by a solid red square. Other related cores referred to in this study are shown by solid red circles.

et al., 1990). The Bohai Sea consists of the Central Basin, Bohai Bay, Liaodong Bay, Laizhou Bay, and Bohai Strait. Two troughs are observed in the north and south at the bottom of the sea, with water depths of 65 and 50 m respectively. The Bohai Strait includes more than 20 islands, with a maximum width of 109 km (Liu et al., 2009). The Laotieshan Channel is the largest channel in the Bohai Strait, measuring 41 km wide and 86 m deep (Liu et al., 2007). Seawater enters the Bohai Sea through the northern Bohai Strait and flows out along the southern margin of the Bohai Sea, where the tidal regime is dominated by semi-diurnal tides (Qin et al., 1990).

The Bohai Sea has received large amounts of sediment from the Yellow River as well as other small rivers, such as the Liao, Luan, and Daling rivers, during its evolution (Qin et al., 2021). These rivers deliver 1.85×10^7 tons/yr of sediment to the sea (Milliman et al., 1987; Wang et al., 2007; Qin et al., 2021). The Bohai basin has been subsiding continuously since the late Oligocene (Allen et al., 1997). The rate of subsidence is estimated to have averaged ~80 m/Ma during the Quaternary, increasing to ~400 m/Ma during the Late Pleistocene owing to the continued active subsidence (Liu et al., 2009; Shi et al., 2016).

MATERIALS AND METHODS

Core YRD-1401 (37.70°N, 118.97°E; length 81.0 m) was drilled in the modern Yellow River delta in 2014 using a rotary drilling method (**Figure 1**). The mean recovery of muddy and sandy sediments was better than 90 and 75%, respectively. The core was split into two sections and preliminarily described in the laboratory. The sediments in core YRD-1401 were sampled for sedimentological, micropalaeontological, and chronological analysis.

Grain-Size Analysis

A total of 464 samples were selected at ~10–20 cm intervals for analyses of grain size, which was measured using a Malvern Mastersizer 2000 laser particle size analyser (Malvern Instruments, United Kingdom) at the Qingdao Institute of Marine Geology, China Geological Survey, Qingdao, China. The organic matter and biogenic carbonate fractions in the samples were removed prior to analysis. Grain-size parameters were determined following Folk and Ward (1957), and the sediment types were described with reference to the classification scheme of Shepard (1954).

Benthic Foraminiferal Analysis

Foraminifera identifications were conducted to assess palaeoenvironmental conditions. In this study, 326 samples were collected from core YRD-1401 at an interval of ~20 cm. These samples were dried at 60°C and then sized through a 63 μm sieve after decanting the organic debris. After sieving, the samples were dried again at 60°C, and the >63 μm fraction of benthic foraminifera was examined under a stereoscopic microscope. The abundances and simple diversity of the foraminifers were calculated with respect to a dry sample size of 50 g. The benthic foraminiferal data of the core have been published elsewhere (Qian et al., 2021).

TABLE 1 | AMS ^{14}C dating results for core YRD-1401.

Depth (m)	Materials	δ ^{13}C (‰)	Conventional ^{14}C age (^{14}C yr BP)	Calibrated age (cal yr BP)		Laboratory code
				Intercept	Range (1σ)	
14.31	Foraminifera	−2.0	2340 ± 30	2006	1904–2108	563798
17.84	Foraminifera	−2.1	4120 ± 30	4228	4123–4345	563799
22.62	Organic	−25.6	8020 ± 40	8888	8783–9007	420267
30.63	Gastropod	−3.0	>43500	—	—	420268
30.75	Gastropod	−8.1	>43500	—	—	420269
39.87	Bivalve mollusc shell fragments	−1.2	>43500	—	—	420270
46.99	Bivalve mollusc shell fragments	−0.5	>43500	—	—	420271
47.07	Gastropod	−2.1	>43500	—	—	420272

Radiocarbon Dating

Eight samples were selected for AMS ^{14}C dating using suitable materials (including benthic foraminifera, organic carbon, bivalve mollusc shells, and gastropods). Dating was performed at the Beta Analytics Laboratory, Miami, Florida, United States. Radiocarbon ages were corrected for the regional marine reservoir effect (△R = −178 ± 50 yr; Southon et al., 2002) and calibrated using Calib Rev. 7.0.4 (Stuiver and Reimer, 1986). The radiocarbon dates are expressed as calibrated calendar years relative to 1950 CE (cal yr BP; or using "ka" in place of "cal kyr BP") with one standard deviation (1σ) uncertainty. In addition, uncalibrated ages are expressed as ^{14}C years BP (^{14}C yr BP). The measured AMS ^{14}C ages are listed in **Table 1**.

Luminescence Dating

Sediments collected for luminescence dating were sampled using opaque plastic cylinders. All OSL samples were prepared under red light in the luminescence dating laboratory of Qinghai Institute of Salt Lakes, Chinese Academy of Sciences, Xining, China.

The middle parts of the sampling cylinders were unexposed and can be used to extract quartz and potassium feldspar (K-feldspar) for determinations of equivalent dose (D_e). To remove carbonates and organic material, the samples were treated with 10% HCl and 30% H_2O_2, respectively. Then, samples were wet-sieved to retrieve 38–63 and 90–125 μm fractions. Heavy liquids with densities of 2.58, 2.62, and 2.75 g/cm^3 were used to separate quartz and K-feldspar grains in the 90–125 μm fraction. K-feldspar grains were treated with 10% HF for 10 min to remove the outer layer irradiated by alpha particles. To remove the feldspar and/or alpha-irradiated layer from quartz grains, the 38–63 and 90–125 μm fractions were treated using H_2SiF_6 (35%) and HF (40%), respectively (Lai and Wintle, 2006). Any fluorides created during the HF etching were removed using 10% HCl, and the purity of the quartz extracts was checked by IR stimulation (Duller, 2003). Quartz grains with obvious IR signals were re-etched with H_2SiF_6 or HF to avoid age underestimation (Lai and Bruckner, 2008).

Water content was measured by weighing the sample before and after drying, assuming an uncertainty of ±5% for all of the samples. Contents of U and Th were determined using inductively coupled plasma–mass spectrometry (ICP–MS), whereas K contents were determined using ICP–optical emission spectroscopy (ICP–OES). The a-value for the 38–63 μm fraction was taken as 0.035 ± 0.003 (Lai et al., 2008). In addition, contents of K and Rb of 12.5 ± 0.5% and 400 ± 100 ppm were assumed for K-feldspar dose rates, respectively (Huntley and Baril, 1997).

The quartz and K-feldspar extracts were mounted on the central part (~0.7 cm diameter) of stainless-steel discs (~0.97 cm diameter) using silicone oil as the fixing agent. All measurements employed a Risø TL/OSL -DA-20 reader equipped with blue diodes (λ = 470 ± 20 nm) and IR diodes (λ = 830 nm). Laboratory irradiation was performed using ^{90}Sr/^{90}Y sources mounted within the reader, with a dose rate of 0.1222 Gy/s. Quartz OSL was detected through a U-340 filter and feldspar IRSL through a combination of BG-39 and coring-759 filters.

RESULTS

Luminescence Characteristics and Reliability of the Ages

Quartz OSL dating in this study employed the SAR-SGC method (Lai and Ou, 2013), which combines Single Aliquot Regeneration (SAR) with Standard Growth Curve (SGC) protocols (Murray and Wintle, 2000; Roberts and Duller, 2004; Lai, 2006). The suitability of the SAR procedure for determinations of D_e was checked using preheat plateau and dose recovery tests. The preheat plateau test was performed on sample OSL-3. Preheat temperatures ranged from 220 to 300°C at a 20°C interval for 10 s, with a heating rate of 5°C/s. The cut-heat temperature was kept constant at 220°C for all measurements. Every four aliquots for each temperature were measured and calculated as the mean values of D_e. A plateau was observed for temperatures from 260 to 300°C (**Figure 2**). In addition, the recycling ratios for different temperatures of sample OSL-3 ranged from 0.95 to 1.03 (lying within the range of 0.9–1.1) (**Figure 2**). According to these results, a preheat temperature of 260°C and a cut-heat of 220°C were employed to measure the D_e of the quartz fraction.

For each sample, an SGC was built using the SAR procedure from 6 aliquots, and the D_e values of 12 additional aliquots were then obtained using this SGC. The D_e value was calculated using the initial 0.64 s integral of the OSL decay curve minus the last 8 s integral. The OSL decay curves and reconstructed dose-response curves for sample YRD-1401-OSL-3 are presented in **Figure 3**. The quartz OSL signals decrease quickly during the first second of

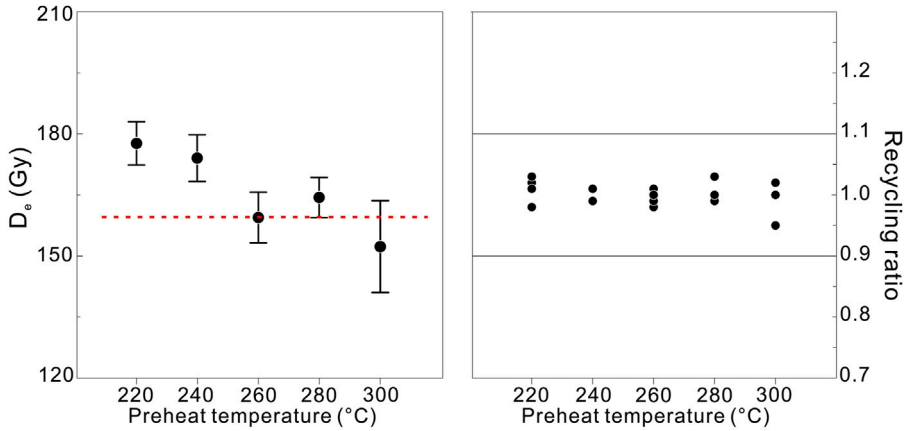

FIGURE 2 | Results of preheating plateau tests and recycling ratios for sample YRD-1401-OSL-3. The equivalent dose (De) of each data point is the mean of four aliquots.

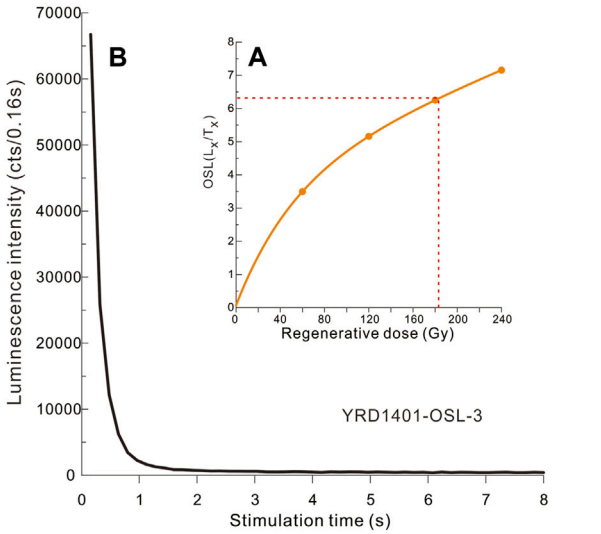

FIGURE 3 | Quartz OSL characteristics of sample YRD-1401-OSL-3. **(A)** growth curve; **(B)** decay curve.

stimulation, indicating that the signal is dominated by the fast component (Singarayer and Bailey, 2003). The values of D_e and ages for each sample were calculated and are listed in **Table 2**.

K-feldspar pIRIR dating utilizing the $pIRIR_{170}$ and $pIRIR_{290}$ signals was used on pre-treated luminescence samples for age estimations. The integrated signal for both pIRIR and $IRSL_{50}$ was calculated from the first 2 s minus the background from the last 40 s. The stimulation time for pIRIR signals used in the current pIRIR SAR protocol was 200 s. The test dose was constant at ~30% of the total measured dose. The $pIRIR_{170}$ decay curve and reconstructed dose-response curves for sample YRD-1401-OSL-4 are presented in **Figure 4**. The IRSL 50°C signal decreases more rapidly than that of $pIRIR_{170}$, which suggests that the latter bleaches more slowly.

Stratigraphic Sequences of Core YRD-1401

Vertical variations in grain size, foraminiferal abundance, simple diversity, and relative abundance of the main foraminiferal species are shown in **Figures 5**, **6**. On the basis of lithofacies characteristics and benthic foraminiferal assemblages, the sedimentary succession in core YRD-1401 can be divided into six stratigraphic units, DU 6 to DU 1 from bottom to top (**Figure 7**).

DU 6 (81.0–51.35 m)

DU 6 is characterized by multiple upward-fining cycles, dominated by yellowish-grey to dark-grey silty sand, sandy silt, and clayey silt, with moderate sorting and tabular cross-bedding (**Figure 8A**). The grain size in this section ranges from 3.5 to 5.5 Φ (**Figure 5**), and medium-grained sands are locally observed. Shell fragments, rusty-brown stains, and carbonaceous spots show a scattered distribution in this unit. According to the benthic foraminiferal assemblages (**Figure 6**), DU 6 can be further divided into three sections.

In the lower section (81.0–68.6 m), the abundances of benthic foraminiferal assemblages range from 1.0×10^3 to 1.0×10^4 species per 50 g, with an average value of 5.0×10^3. The simple diversities vary between 2 and 16, with an average value of 8. The assemblages are dominated alternately by euryhaline species (e.g., *Ammonia. beccarii* variabilis, *Elphidium magellanicum*, and *Cribrononion subincertum*) and shallow-water marine species (e.g., *Protelphidium tuberculatum*, *Buccella frigidum*, *Elphidium advenum*, and *Quinqueloculina seminula*). In the middle section (68.6–57.6 m), however, foraminifera occur sporadically, with relatively low abundances and simple diversities (most values being $<1.2 \times 10^3$ and 10, respectively). The assemblages are dominated by *A. beccarii* vars., and the relative content of brackish water species increases (e.g., *Haynesina germanica* and *Pseudononionella* variabilis) compared with the lower section. The values of average abundance and simple diversity of foraminiferal assemblages in the uppermost part of DU 6 (51.4–57.8 m) are 2.4×10^3 and 9, respectively, which are

TABLE 2 | OSL dating results for core YRD-1401.

Sample no	Grain size (μm)	Depth (m)	U (ppm)	Th (ppm)	K (%)	Water (%)	Number of aliquots	Overdispersion	D_e (Gy)	Dose rate (Gy/ka)	Age (ka)
YRD-1401-OSL-1	38–63	19.40	1.59 ± 0.3	7.96 ± 0.5	1.79 ± 0.03	16 ± 5	18	0.07 ± 0.02	15.7 ± 0.3	2.47 ± 0.12	6.4 ± 0.3
YRD-1401-OSL-1(f)	38–63	19.40	1.59 ± 0.3	7.96 ± 0.5	1.79 ± 0.03	16 ± 5	6	—	53.7 ± 0.4	2.65 ± 0.12	20.2 ± 0.9
YRD-1401-OSL-2	90–125	29.20	1.05 ± 0.2	4.6 ± 0.4	1.87 ± 0.03	16 ± 5	18	0.20 ± 0.01	98.4 ± 11.2	2.09 ± 0.1	47.0 ± 5.9
YRD-1401-OSL-3	38–63	33.20	1.64 ± 0.3	7.19 ± 0.5	1.91 ± 0.03	18 ± 5	18	0.14 ± 0.02	156.7 ± 0.5	2.39 ± 0.11	65.5 ± 3.1
YRD-1401-OSL-4	38–63	37.30	1.23 ± 0.2	5.46 ± 0.4	2.03 ± 0.04	16 ± 5	18	0.28 ± 0.05	147.3 ± 9.9	2.34 ± 0.11	63.0 ± 5.2
YRD-1401-OSL-4(f)	38–63	37.30	1.23 ± 0.2	5.46 ± 0.4	2.03 ± 0.04	16 ± 5	4	—	185.0 ± 9.4	2.51 ± 0.11	73.8 ± 4.9
YRD-1401-OSL-5	38–63	40.40	1.79 ± 0.3	9.06 ± 0.5	1.55 ± 0.03	19 ± 5	18	—	232 ± 13	2.21 ± 0.1	105 ± 8
YRD-1401-OSL-6	38–63	46.40	1.85 ± 0.3	8.14 ± 0.5	2.17 ± 0.04	18 ± 5	18	—	220 ± 11	2.72 ± 0.13	81.0 ± 5.5
YRD-1401-OSL-7	38–63	53.60	1.24 ± 0.2	6.46 ± 0.4	2.14 ± 0.04	16 ± 5	17	—	294 ± 15	2.5 ± 0.12	118 ± 8
YRD-1401-OSL-8	38–63	58.60	1.45 ± 0.2	7.02 ± 0.5	1.84 ± 0.03	18 ± 5	17	—	289 ± 14	2.27 ± 0.1	127 ± 8
YRD-1401-OSL-9	38–63	62.30	0.83 ± 0.2	2.88 ± 0.3	2.34 ± 0.04	18 ± 5	18	—	348 ± 8	2.31 ± 0.12	151 ± 8
YRD-1401-OSL-10	38–63	65.00	0.8 ± 0.2	3.54 ± 0.3	2.38 ± 0.04	18 ± 5	18	—	294 ± 19	2.39 ± 0.12	123 ± 10
YRD-1401-OSL-10(f)	38–63	65.00	0.8 ± 0.2	3.54 ± 0.3	2.38 ± 0.04	18 ± 5	5	—	583.0 ± 26.8	2.52 ± 0.11	236.1 ± 14.9
YRD-1401-OSL-11	38–63	67.20	1.03 ± 0.2	5.77 ± 0.4	2.21 ± 0.04	17 ± 5	17	—	359 ± 19	2.46 ± 0.12	146 ± 10
YRD-1401-OSL-12	38–63	70.10	1.0 ± 0.2	5.18 ± 0.4	2.34 ± 0.04	16 ± 5	17	—	375 ± 23	2.53 ± 0.12	148 ± 11
YRD-1401-OSL-14	38–63	78.80	1.54 ± 0.2	6.54 ± 0.4	2.24 ± 0.03	16 ± 5	18	—	409 ± 11	2.65 ± 0.28	154 ± 17
YRD-1401-OSL-15	38–63	80.50	1.13 ± 0.2	5.8 ± 0.4	2.31 ± 0.04	18 ± 5	17	—	402 ± 27	2.54 ± 0.12	159 ± 13
YRD-1401-OSL-15(f)	38–63	80.50	1.13 ± 0.2	5.8 ± 0.4	2.31 ± 0.04	18 ± 5	6	—	1000.0 ± 25.9	2.67 ± 0.11	375.1 ± 18.7

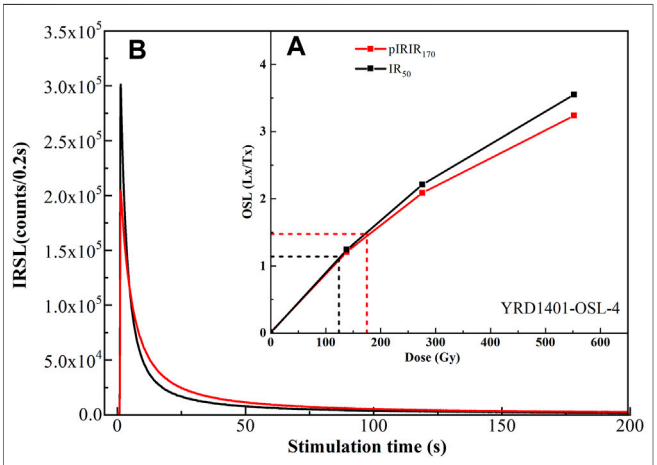

FIGURE 4 | IRSL signals of sample YRD-1401-OSL-4. **(A)** growth curves; **(B)** decay curves.

dominated by euryhaline species such as *A. beccarii* vars. and *C. subincertum*.

According to lithofacies and benthic foraminiferal assemblages, DU 6 is interpreted as tidally influenced river deposits in an estuarine environment. The rusty-brown stains and carbonaceous spots scattered in this unit are indicative of subaerial exposure, typical of tidal-river environments. Sandbeds with basal erosional surfaces, fining-upward trends, and cross-bedding are indicative of tidal-channel deposition (Reineck and Singh, 1980).

DU 5 (51.35–37.64 m)

The sediments in DU 5 are composed of grey and yellow silt (**Figure 8B**) and are finer than those of DU 6. Tabular cross-bedding and upward-fining cycles are observed, and the grain size ranges from 5.5 to 6.5 Φ (**Figure 5**). The abundances of benthic foraminifera vary from 2.8×10^3 to 1.0×10^5 species per 50 g, and the simple diversity value is 11. These are the maximum values of abundance and simple diversity in core YRD-1401. The

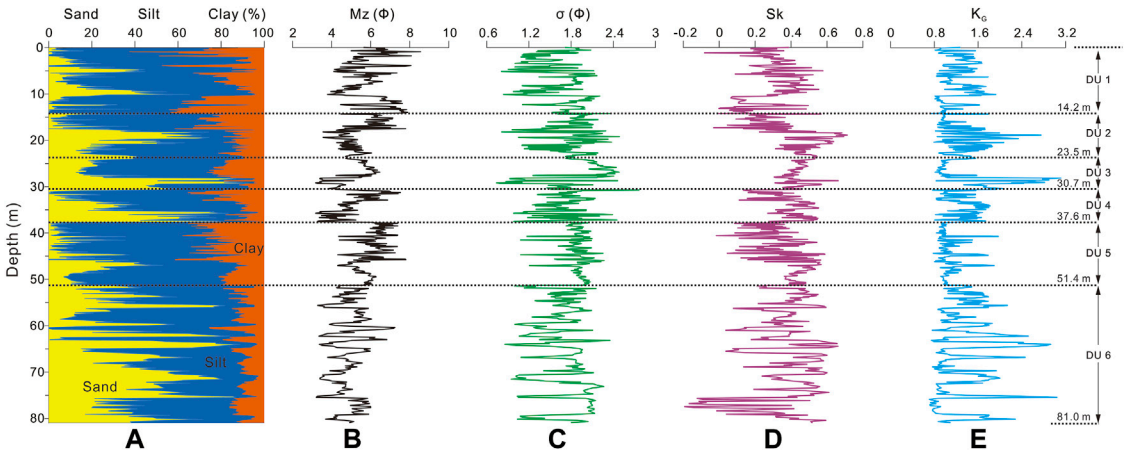

FIGURE 5 | Down-core variations in grain-size composition **(A)** and grain-size parameters **(B–E)** of core YRD-1401. Mz, mean grain size; σ, sorting coefficient; Sk, skewness; KG, kurtosis. DU 1–DU 6, depositional units.

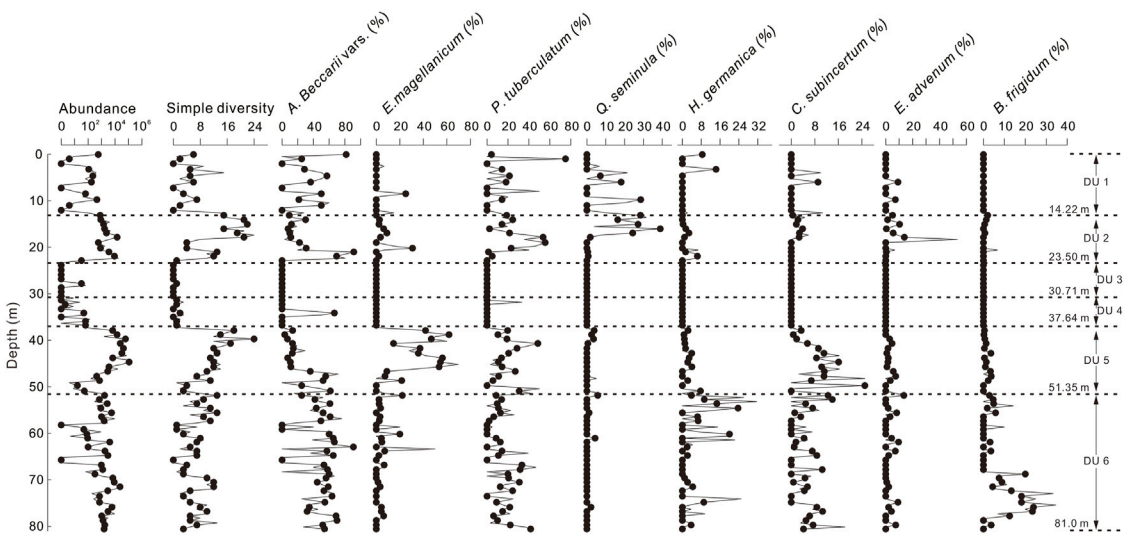

FIGURE 6 | Down-core variations in benthic foraminiferal abundance, simple diversity, and relative abundance of the main foraminiferal species in coreYRD-1401.

assemblages are dominated by shallow-water euryhaline species (mainly in the lower interval) and shallow-water marine species (in the upper interval), with a boundary between the two intervals at 47.03 m (**Figure 6**).

DU 5 is inferred to represent deposition in a tidal-flat to a shallow-subtidal environment, which is supported by the lithofacies characteristics and down-core changes in benthic foraminiferal assemblages.

DU 4 (37.64–30.71 m)

DU 4 is characterized by yellow and greyish-yellow fine sand, sandy silt, and clayey silt (**Figure 8C**), with some rusty-brown stains and tidal bedding. Upward-fining depositional cycles and moderate to poor sorting are common, with the values of mean grain size ranging between 3.9 and 5.9 Φ. The abundances of benthic foraminiferal assemblages in DU 4 are notably lower compared with DU 5, as are the simple diversities (**Figure 6**). Benthic foraminifers (average = 32 species per 50 g) occur sporadically and are dominated by *A. beccarii* vars. and *P. tuberculatum*.

According to the low abundance and sporadic distribution of benthic foraminifera, the common tidal bedding, and rusty-brown stains, DU 4 is interpreted as tidal-flat deposits of an oxidizing and/or subaerial environment.

DU 3 (30.71–23.50 m)

A dual structure, with fine and silty sand in the lower section and silt in the upper section (**Figure 8D**), is observed in DU 3. Tabular cross-bedding, strong bioturbation, and rusty-brown stains are

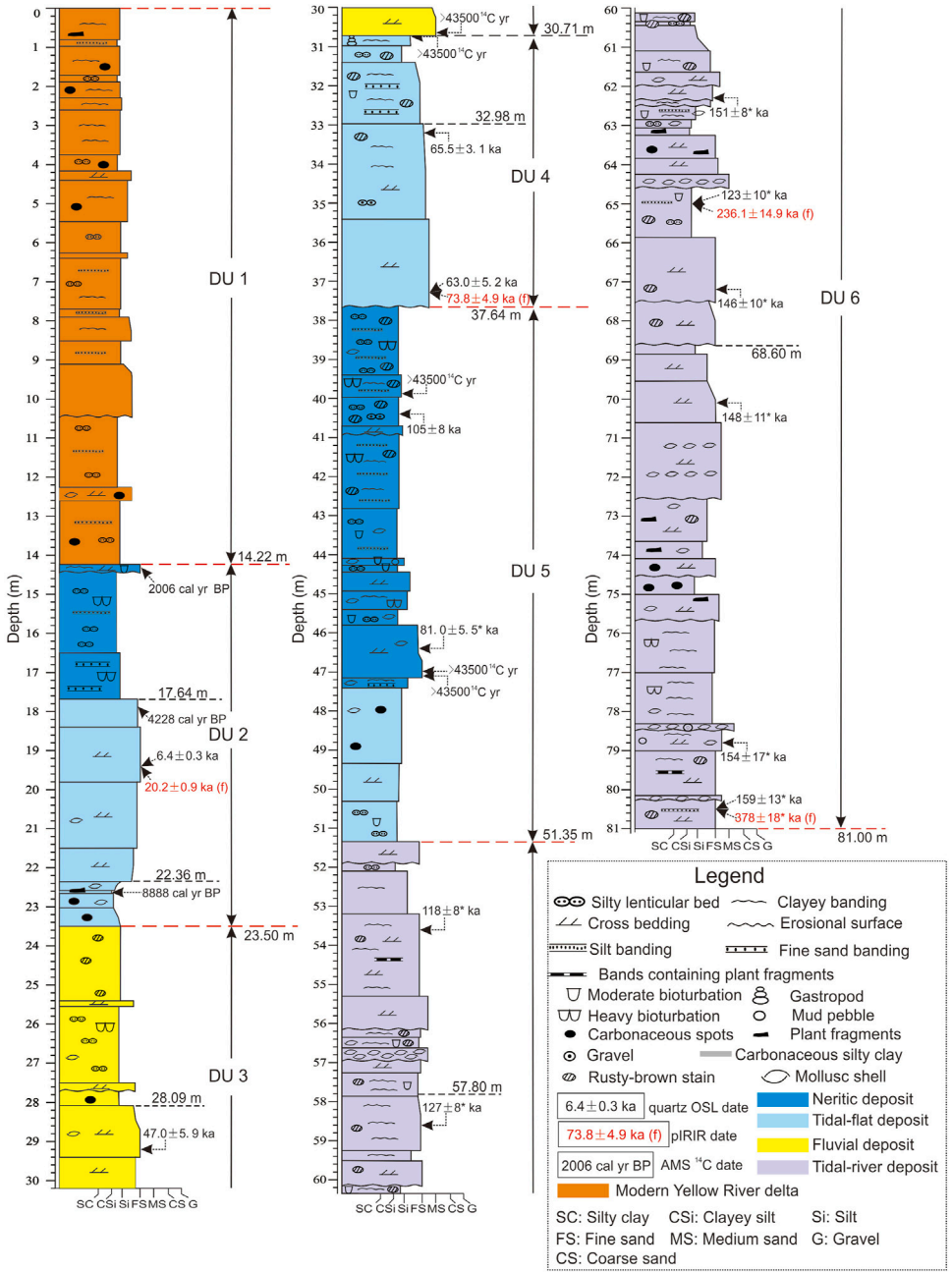

FIGURE 7 | Lithological log of core YRD-1401, with calibrated ^{14}C and OSL ages.

common, and the sediments show poor sorting. A few foraminifera in this unit may have been reworked and/or transported, as inferred from their abraded and oxidized characteristics.

Given the lithology and benthic foraminiferal characteristics, this unit is interpreted as fluvial deposits.

DU 2 (23.50–14.22 m)

DU 2 can be further divided into three subunits. The lower subunit (23.50–22.36 m) consists of greyish-yellow to dark-grey clayey silt, with numerous carbonaceous spots and scattered shell fragments. In this subunit, the benthic foraminiferal assemblage is dominated by brackish water species (*H. germanica*), and the average values of abundance and simple diversity are 992 species per 50 g and 1, respectively. The middle submit (22.36–17.64 m) is composed predominantly of fine sand and silty sand, with some clayey bands. Tabular cross-bedding is common, and scattered shell fragments are observed. The benthic foraminiferal assemblage is dominated by *A. beccarii* vars., *P. tuberculatum, E. advenum*, and *E. magellanicum*. An increase in the abundance

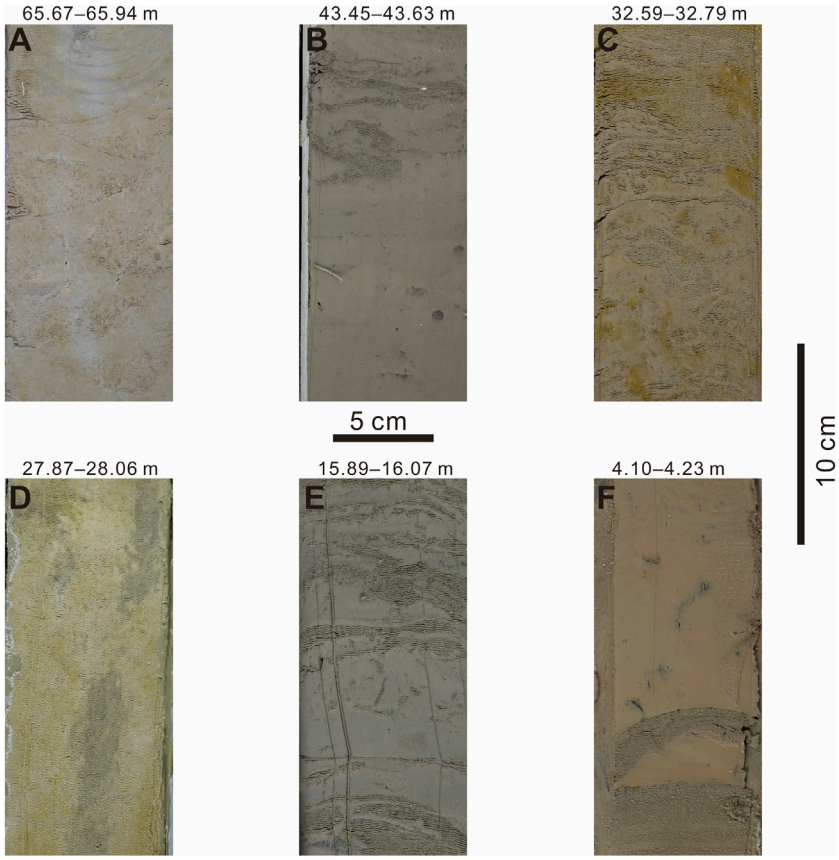

FIGURE 8 | Photographs of representative sedimentary facies in core YRD-1401. **(A)** 65.67–65.94 m core depth (DU 6): yellowish-grey fine sands with moderate sorting and tabular cross-bedding. **(B)** 43.55–43.73 m (DU 5): dark-grey clayey silt, with silty bands, lenses, and shell fragments. **(C)** 32.59–32.79 m (DU 4): greyish-yellow silty sand interbedded with sandy silt and clayey silt, with rusty-brown stains and strong bioturbation. **(D)** 27.87–28.06 m (DU 3): greyish-yellow silt, with carbonaceous spots. **(E)** 15.89–16.07 m (DU 2): dark-grey silt and clayey silt, with silty lenses and strong bioturbation. **(F)** 4.10–4.23 m (DU 1): yellow to greyish-yellow sandy silt and silt, with carbonaceous spots and clayey bands.

of benthic foraminifera (averaging 5.0×10^3 species per 50 g) is observed. The uppermost submit (17.64–14.42 m) is characterized by silt and clayey silt, with silty lenses and strong bioturbation (**Figure 8E**). A yellowish-gray fine sand layer (~20 cm thick) is found at 14.4–14.2 m and shows moderate sorting and tabular cross-bedding. The average values of foraminiferal abundance and simple diversity in this subunit are 4.3×10^3 species per 50 g and 21. The abundances of euryhaline and shallow-water species are lower and higher, respectively, compared with the middle submit.

DU 2 is interpreted to have been deposited from the middle to late Holocene in a coastal to nearshore shelf environment, as evidenced by the strong bioturbation and high abundances of foraminifera.

DU 1 (14.22–0 m)

DU 1 is composed of yellow to greyish-yellow sandy silt and silt. Tidal bedding, molluscan shell fragments, carbonaceous spots, and rusty-brown speckles occur locally, as well as some clayey bands (**Figure 8F**).

The benthic foraminiferal assemblage of DU 1 exhibits low abundances and low diversities. The abundance averages 581 species per 50 g, and the diversity averages 6. The assemblage is dominated by euryhaline and shallow-water marine species, such as *A. beccarii* vars., *P. tuberculatum*, and *Q. seminula*.

According to the absence of bioturbation, and the low abundances and low simple diversities of benthic foraminifera, DU 1 is interpreted as deposits of the modern Yellow River delta since 1855, when the Yellow River shifted its main course and discharged into the Bohai Sea (Alexander et al., 1991).

DISCUSSION

Chronostratigraphic Framework of the Core YRD-1401

We established the chronostratigraphic framework of the depositional units in core YRD-1401 using the dating results of quartz OSL, feldspar pIRIR, and AMS ^{14}C. As mentioned above, radiocarbon and OSL dating have their particular advantages and limitations. In this study, ^{14}C is regarded as the preferred method for young dates and yields reliable and accurate ages for Holocene sediments. OSL performs well and outperforms ^{14}C dating for the old (>25 ka) sediments. Considering the saturation levels of quartz

signals, ages obtained by quartz OSL dating can be regarded as reliable for pre-Holocene sediments when the D_e value is less than *ca.* 230 Gy (Lai, 2010). However, only minimum ages can be provided when the quartz signals are greater than *ca.* 230 Gy. Therefore, for samples that exceed the upper limit of quartz OSL dating, the results derived from pIRIR dating may be more accurate.

For DU 6, eight samples yielded the quartz OSL ages between 159 ± 13 and 118 ± 8 ka, which lie beyond the dating limit (with respect to the above-mentioned D_e threshold value) and are, therefore, regarded as minimum ages of the sediments (Wintle and Murray, 2006; Lai, 2010). To further constrain the timing of DU 6, the pIRIR protocol with an elevated temperature stimulation of 290°C was used. One infinite $pIRIR_{290}$ age [YRD-1401-OSL-15 (f)] of >378 ka (minimum age: 378 ± 18 ka) at 80.50 m was determined from the basal part of DU 6, for which the value of D_e is greater than 1000 Gy. Another $pIRIR_{290}$ age [YRD-1401-OSL-10 (f)] of 236.1 ± 14.9 ka obtained at ~65.00 m corresponds to MIS 7. Therefore, we suggest that DU 6 was formed during MIS 6 or even older.

Three AMS ^{14}C dates for DU 5 (47.07–39.87 m) are beyond the age limit of radiocarbon dating (>43.5 kyr BP). Two OSL dates of 105.0 ± 8.0 and 81.0 ± 5.5 ka were obtained from this unit, indicating that it was deposited during MIS 5.

In DU 4, an AMS^{14}C date for the upper part of DU 4 (at 30.75 m) is beyond the limit of the radiocarbon method, and only an infinite age of 43.5 ka can be given. In addition, the stratigraphic interval of DU 4 was dated between 64.1 ± 5.1 and 63.0 ± 5.2 ka using quartz OSL dating, which corresponds to early MIS 3 considering the age error. These ages were cross-checked using the pIRIR protocol with an elevated temperature stimulation of 170°C. The aliquots of sample YRD-1401-OSL-4 were bleached for 56 h under sunlight (8 h per day for 7 days) to determine the residual dose, which has an important influence on pIRIR dating. After subtraction of the residual dose (46.1 Gy), the resultant $pIRIR_{170}$ age (YRD-1401-OSL-4 (f)) of 73.8 ± 4.9 ka is older than the quartz OSL age (63.0 ± 5.2 ka) at the same depth of 37.30 m. This age inconsistency for the same sample may have been caused by a residual signal that is unbleached or hard to bleach by pIRIR dating, as the natural bleaching process in coastal areas is uncertain (Li et al., 2014; Li et al., 2018; Long et al., 2019). Within age uncertainties, the timing of deposition of DU 4 corresponds to early MIS 3.

An OSL age for YRD-1401-OSL-2 of 47.5 ± 5.9 ka was obtained at 29.20 m, and an AMS ^{14}C date (>43.5 kyr BP) for the lower part of DU 3 is beyond the age limit of radiocarbon dating, indicating that DU 3 was deposited during late MIS 3.

In DU 2, three samples were selected and dated at 2006, 4228, and 8888 cal yr BP using AMS ^{14}C dating. An OSL age of 6.3 ± 0.5 ka obtained at 19.4 m, together with ^{14}C results, constrains this unit to the Holocene. According to the progradation history of the Yellow River delta (Xue, 1993; Saito et al., 2000) and the lithology and stratigraphic position of DU 1, DU 1 is interpreted as deltaic deposits of the modern Yellow River.

Analysis and Correlation of Sedimentary Strata in the Bohai Sea

The sedimentary sequences recorded in the coastal areas of eastern China vary with respect to sediment supply, stratigraphic completeness, and core locations (Liu et al., 2016). Therefore, the sedimentary evolution of the Bohai Sea is best established by using sedimentary records of multiple cores. Here, we use the results from core YRD-1401, together with results from other cores examined by previous studies, to make a regional comparison of sedimentary strata deposited since *ca.* 200 ka in the coastal areas of Bohai Sea.

A comparison of the stratigraphic sequence of core YRD-1401 with that of other cores, including LZK06 (Li et al., 2019), BT113 (Chen et al., 2012), YRD-1101 (Liu et al., 2016), Lz908 (Yi et al., 2012), and YRD-1402 (Zhang et al., 2016), are shown in **Figure 9**. The sedimentary sequences can be divided into four depositional units, designated L4 to L1 in ascending order.

Sedimentary sequences in L4 were deposited prior to 130 ka. Fluvial and tidal-river sedimentation prevailed in Liaodong Bay (LZK06 core) and the western coast of the Bohai Sea (e.g., cores BT113, YRD-1101, and YRD-1401). L4 in Laizhou Bay is dominated by alternations of sediments deposited in tidal-flat and fluvial environments (core Lz908). All of the quartz OSL ages for this unit are beyond the upper limit of this dating method and are presented as minimum ages of the sediments. Most of the pIRIR ages vary between 260 and 130 ka, with IRSL signals in some ages being saturated. Considering one infinite $pIRIR_{290}$ age of >378 ka and another $pIRIR_{290}$ age of 236.1 ± 14.9 ka for core YRD-1401 (**Figure 7**), it is speculated that fluvial and tidal-river environments prevailed in the Bohai Sea during MIS 6 or earlier.

L3 corresponds to sedimentary sequences that formed between 130 and 60 ka and show wide differences between the compared cores. In cores BT113 and YRD-1101, this unit consists mainly of neritic and fluvial deposits, indicating sea-level fluctuation in the Bohai Sea during MIS 5, and these deposits are consistent with those in the Pearl River delta (Fu et al., 2020). In other cores, this unit is dominated by neritic and tidal-flat deposits, with the OSL ages falling in the 100–60 ka range. The chronology and lithology demonstrate that alternating marine and terrestrial environments on the northern and western coasts of the Bohai Sea and tidal-flat environments on the south coast of the Bohai Sea occurred during early MIS 3–MIS 5.

Unit L2 is dominated by fluvial-facies sediments and is estimated to have formed from *ca.* 60 to 10 ka. OSL ages constrained the fluvial sediments to mid-MIS 3–MIS 2, including cores BT113, YRD-1101, YRD-1402, and YRD-1401. However, some marine-influenced sediments in cores LZK06 and Lz908 are also observed in cores LZK06 and Lz908 and have OSL ages of *ca.* 40 ka.

The sedimentary sequences of L1 were deposited during the Holocene and are characterized by neritic and tidal-flat deposits associated with sea-level rise. Dating results of ^{14}C and OSL methods suggest that this unit was affected by the Holocene transgression in the Bohai Sea (e.g., Yi et al., 2012; Liu et al., 2016). L1 also contains Yellow River sediments deposited since AD 11 in the modern Yellow River delta.

Sedimentary Record of MIS 3 in the Bohai Sea

Reconstruction of sea-level change and transgression history over the past 200 ka for the Bohai Sea is challenging because of

discrepancies among dating results, and it is still unclear whether the seawater covered the present coastal areas of the Bohai Sea during MIS 3. Previous studies of stratigraphic imprints and chronology have elucidated transgression histories in the coastal to shelf areas of eastern China (Qin and Zhao, 1985; Xu et al., 2011), where three marine units (i.e., M-3, M-2, and M-1) have been identified. It is well established that M-1 was deposited during the Holocene (e.g., Zhang et al., 2016; Li et al., 2019), as constrained by numerous dating results. However, it remains unclear whether the second transgression (M-2) occurred during MIS 3 or MIS 5, despite considerable research carried out on this problem (Li et al., 2019; Gao et al., 2021). Put another way, it is uncertain whether the MIS 3 transgression occurred in the coastal areas of eastern China.

Accurate and consistent chronology is the key to solving this problem. Previous studies have determined age for M-2 of *ca*. 40 ka using ^{14}C dating of shells, wood, and benthic foraminifera (e.g., Hanebuth et al., 2006; Shang et al., 2018), corresponding to middle to late MIS 3. However, these dating materials are vulnerable to contamination by new carbon, which would lead to an underestimation of radioactive ages (Pigati et al., 2007). For example, the apparent age of one old sample (beyond the upper limit of ^{14}C dating) mixed with 1% new carbon will give an age of 38 ka (Aitken, 1990). ^{14}C ages older than 35 ka should be treated with caution, and additional dating methods are needed to verify (Gao et al., 2019). The M-2 deposits, originally dated as MIS 3 using ^{14}C dating (e.g., Zhao et al., 1978; Hanebuth et al., 2006; Liu et al., 2009; Wang et al., 2014; Shang et al., 2018), have been re-evaluated to MIS 5 or even older based on U-series and OSL dating results (Wang et al., 2021).

After re-examination of the available geological and geochronological data, Chen et al. (2012) and Gao et al. (2019) concluded that there was no reliable evidence for the deposition of marine sediments during MIS 3 in the Yangtze River delta and the western Bohai Sea, And it was presumed that all OSL ages for M-2 would belong to MIS 5. However, Yao et al. (2010) identified a transgression layer with abundant benthic foraminifera in core Lz908. In a subsequent study, radiocarbon dates and OSL ages constrained this transgression event to MIS 5–3 (Yi et al., 2012). Moreover, a more recent study showed that M-2 corresponds to MIS 3 and did not detect MIS 5 marine deposits in the northern coast of the Bohai Sea (Li et al., 2019). In core YRD-1401, tidal-flat deposits are revealed in DU 4, as inferred from low-abundance and sporadic benthic foraminifera, tidal bedding, and rusty-brown stains. OSL ages of 65.5 ± 3.1 and 63.0 ± 5.2 ka were obtained from this unit in the present study, which correspond to early MIS 3. Considering the saturated dose of 230–150 Gy (i.e., a quartz OSL age of *ca*. 70 ka) (Lai et al., 2010), it is necessary to further constrain the timing of formation of these tidal-flat deposits using pIRIR dating. A $pIRIR_{170}$ age of 73.8 ± 4.9 ka was obtained for sample YRD-1401-OSL-4, which is older than its quartz OSL age. Given the complex and uncertain bleaching process of IRSL signals in coastal areas, the residual doses of samples from such areas may be large, and therefore the $pIRIR_{170}$ age of 73.8 ± 4.9 ka of sample YRD-1401-OSL-4 may have been slightly overestimated. Therefore, we argue that the quartz OSL age and $pIRIR_{170}$ age of sample YRD-1401-OSL-4 are consisting within error ranges and correspond to early MIS 3 (*ca*. 60 ka).

It has been suggested that marine transgressions in the Bohai Sea are influenced by multiple factors, including sea-level change, sediment input, and palaeotopography (Liu et al., 2009). The Bohai Sea is separated from the Yellow Sea by the Miaodao Islands Uplift (**Figure 1**), which has blocked the passage of seawater from the Yellow Sea into the Bohai Sea since its uplift during the late Mesozoic (Yi et al., 2016). However, as a result of subsequent subsidence of the Miaodao Island Uplift, regional seawater has entered the Bohai Sea since the late Pleistocene (Liu et al., 2016). Hence, it is necessary to reconstruct the paleo sea level and establish whether seawater could have flooded the Miaodao Islands Uplift during early MIS 3. Palaeo sea level is commonly represented by the elevation of associated tidal-flat deposits. The Bohai Sea has been in a state of continuous subsidence over the past 6 Ma, at a rate of 0.12–0.50 m/ka (Guo et al., 2007; Liu et al., 2016). Considering that the rate of subsidence has decreased substantially during the late Pleistocene, it is estimated that the amount of tectonic subsidence in the Bohai Sea since early MIS 3 is ~7.2 m, using the minimum subsidence rate (0.12 m/ka). In addition, the reconstruction of the palaeo sea level could be affected by sediment compaction (Qin et al., 2020). In this study, the sediments in YRD-1the 401 core are composed of silty sand, which has a limited effect on compaction. Therefore, the thickness of compaction is assessed at ~1 m. The tidal-flat deposits at 37.64–30.71 m in core YRD-1401 correspond to early MIS 3. The sea level during early MIS 3 is estimated to have ranged from 26.8 to 19.9 m below the present sea level in the Bohai Sea when the elevation of the core (+2.64 m), tectonic subsidence (7.2 m), and post-deposition compaction (~1 m) are taken into account. An analogous high stand of sea level has been reported in other areas, including the Yangtze River and Red River deltas (Hanebuth et al., 2006; Pico et al., 2016; Shang et al., 2018). According to the rate of tectonic subsidence (0.12–0.50 m/ka), the subsidence of the Miaodao Islands Uplift since early MIS 3 (*ca*. 60 ka) is between 7.2 and ~30 m. The water depth at the bottom of the southern trough of the Miaodao Islands Uplift and the maximum depth of the Laotieshan channel would have exceeded 20 and 50 m, respectively, which would have enabled the seawater to enter the Bohai Sea *via* the Miaodao Islands Uplift during early MIS 3.

Furthermore, the southern Bohai Sea has been in a stage of continuous subsidence since the late Quaternary, which would have provided sedimentary accommodation space for marine transgressions. However, the MIS 5 transgression was weak and/or absent in the northern Bohai Sea because the depositional elevation in the northern Bohai Sea may be higher than the sea level (Li et al., 2019; Wang et al., 2020). Moreover, some researchers have ascribed the unexpectedly strong transgression during MIS 3 in the marginal seas off eastern China to continuous tectonic subsidence since MIS 5 (e.g., Yan et al., 2006; Wang et al., 2013). However, our results show that the MIS 3 transgression along the southwestern coast of the Bohai Sea occurred only in the early part of this MIS and that a tidal-flat environment prevailed. The foraminiferal assemblages and abundances (**Figure 6**) and lithologic characteristics of rusty-brown stains and tidal bedding (**Figure 8**) show that the marine transgression during MIS 3 was

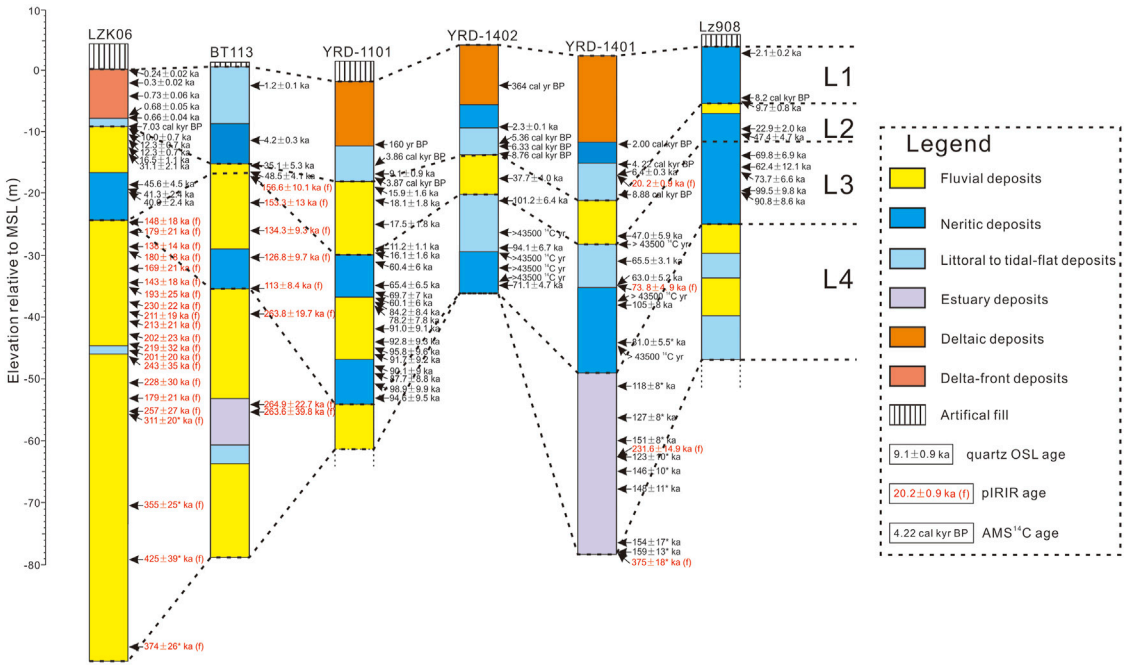

FIGURE 9 | Stratigraphic correlations between cores from the Bohai Sea, with sedimentary facies and ages.

weaker than that during MIS 5, despite the continuing subsidence. This contradiction between the intensity of transgression and sea-level change is likely to have been caused by the lack of a clear and reliable chronological framework rather than uncertainty regarding the amount of tectonic subsidence.

Finally, the basis of the record of marine transgressions is stratigraphic completeness (Yi et al., 2012; Liu et al., 2016). During the late Quaternary, erosion occurred with increasing frequency in the complex sedimentary environments of coastal and nearshore areas. The transportation of sediments in channels and periods of erosions are marked by unconformities in stratigraphic records (Straub et al., 2020). In fact, the high degree of instability of the climate and sea-level fluctuations during the Last Glacial, produced extreme erosion events, including the channelization of rivers into the underlying sediments. During the Last Glacial Maximum, a large number of palaeo river channels developed and incised the coastal to shelf areas, with a sea level of approximately 130 m below the present sea level (Liu et al., 2010). These palaeo channels were filled and/or erased by subsequent transgression, with deposits being only partially preserved in the geological record (Fagherazzi et al., 2008). As a result, the study of sedimentary environments and the associated marine transgression during MIS 3 requires detailed analyses of successive sedimentary facies and a reliable chronological framework.

Sedimentary Evolution of the Bohai Sea Since 200 ka

The sedimentary characteristics and chronostratigraphic framework of core YRD-1401, together with other cores examined by previous studies, enable the sedimentary evolution of the Bohai Sea to be understood from the perspective of sea-level change, sediment supply, and geomorphology over the last 200 ka.

The Miaodao Islands Uplift has existed since the late Mesozoic and has played an important role in the sedimentary evolution in the Bohai Sea (Yi et al., 2016). Several weak transgressions are recorded in the Bohai Sea at *ca.* 0.83 Ma and ascribed to the tectonic subsidence of the Miaodao Islands Uplift (Liu et al., 2016). The climate was relatively warm and wet during MIS 7, although it was interrupted by a cold substage (MIS 7d) and did not reach the peak of that of MIS 5 and the Holocene (Rowe et al., 2014; Columbu et al., 2019). Subsequently, the global sea level fell by 120–130 m during MIS 6, which was characterized by a cold and dry climate (Antonioli et al., 2004). The deposits of DU 6 suggest that in the study area, a tidal-river environment prevailed from MIS 7 to MIS 6. The rusty-brown stains and carbonaceous spots observed in DU 6 are interpreted as representing subaerial exposure. The sand beds with basal erosional surfaces and cross-bedding are indicative of tidal-channel deposition, as indicated by the relatively low abundance and simple diversity of foraminifera as well as by the foraminiferal assemblages, which are dominated by low-salinity species. In addition, high abundances of *H.germanica* in the benthic foraminiferal assemblages were observed in core YRD-1401 (57.80–51.35 m), which suggests that strong tidal currents occurred during MIS 7 to MIS 6 (Hayward and Hollis, 1994).

Following MIS 6, the global sea level rose and reached its peak during MIS 5e (Shackleton, 1987), and marine deposits were ubiquitous in the coastal to shelf areas of eastern China. This large-scale transgression in the South Yellow Sea is recorded by *Asterorotalia* spp. and involved a cold-water mass in the central South Yellow Sea (Wang et al., 1981; Yang et al., 1998). During

MIS 5, neritic deposits were common in the Bohai Sea, with OSL ages of 100–90 ka (Liu et al., 2016). This view is further confirmed by the deposits of DU 5. The abundance and simple diversity of foraminifera both reach their highest values in this unit in core YRD-1401, and the assemblages are dominated by shallow-water marine/euryhaline species, which suggests that a strong transgression occurred in the Bohai Sea during MIS 5. However, sedimentary evidence from the Pearl River delta and Yangtze River delta shows that sea level fluctuated and these areas were not covered by seawater continuously during MIS 5 (Zhao et al., 2008; Fu et al., 2020). These sea-level fluctuations are also revealed on western coast of the Bohai Sea, where the sedimentary sequences contain alternations of tidal-flat and neritic deposits and are intercalated with fluvial and tidal-river deposits (**Figure 9**). It is worth noting that the completeness of sedimentary sequences in some cores is poor, which could be a result of subsequent river erosion and/or scouring by transgressive processes. In addition, some factors including high elevation in palaeotopography and sediment discharge during MIS 5 seem to have been unfavorable for the development of marine deposits (Wang and Tian, 1999; Wang et al., 2008). For example, the marine sedimentary interval of MIS 5 is not observed in Liaodong Bay (Li et al., 2019) due to its high elevation in palaeotopography (Wang et al., 2020).

During MIS 4, the sea level fell to ~80 to ~90 m below the present sea level, and rivers developed in coastal areas (Chappell et al., 1996; Liu et al., 2010). With the development of rivers, fluvial processes further eroded late Quaternary strata in coastal to shelf areas (Fagherazzi et al., 2008). The MIS 3 transgression along the southwestern coast of the Bohai Sea occurred in early MIS 3, when a tidal-flat environment developed on the southwestern coast of the Bohai Sea. During middle MIS 3 to MIS 2, the lowered sea level exposed the coastal to shelf areas, and a terrestrial environment prevailed (Zhou et al., 2014; Liu et al., 2016).

A peat layer underlying DU 2 at a depth of 22.62 m yielded an age of 8888 cal yr BP in this study, indicating a prevailing coastal marsh sedimentary environment during 9000–8000 yr BP in the Bohai Sea (Qin et al., 1990; Saito et al., 2000). Later, coastal marshes were quickly inundated by seawater, and the sedimentary environment changed from terrestrial (fluvial or lacustrine) to coastal marine (Qiao et al., 2011). During the maximum Holocene transgression, the western coastline of the Bohai Sea lay 50–90 km west of the present coastline (Liu et al., 2016). The ages (including OSL ages and AMS^{14}C ages) and foraminiferal assemblages of DU 2 suggest that a marine transgression (i.e., M-1) occurred along the southern Bohai Sea during the Holocene.

CONCLUSION

OSL dating and lithological of core YRD-1401 from the Yellow River delta were used to establish the late Quaternary sedimentary evolution of the southwestern coast of the Bohai Sea. The main conclusions of the study are as follows:

(1) A weak transgression (dominated by tidal-flat deposits) is inferred along the southwestern coast of the Bohai Sea during early MIS 3 and was weaker than the transgression of MIS 5.
(2) The sea level during early MIS 3 is estimated to have ranged from 26.8 to 19.87 m below the present sea level in the Bohai Sea, which allowed seawater to enter the Bohai Sea *via* the Miaodao Islands Uplift during this period.
(3) The measured luminescence ages and foraminiferal assemblages indicate that M-3 was likely formed during MIS 5 and that a tidal-river environment prevailed on the southwestern coast of the Bohai Sea during MIS 6 or earlier.

DATA AVAILABILITY STATEMENT

The original contributions presented in the study are included in the article/Supplementary Material, further inquiries can be directed to the corresponding authors.

AUTHOR CONTRIBUTIONS

XZ and JL designed the study. XZ wrote the manuscript. XZ, YW, and TC analyzed the data related to the OSL chronology. SQ analyzed the data of microfossils. MA helped to revise the manuscript and give some useful suggestions. All authors contributed to the article and approved the submitted version.

FUNDING

This research was funded by the National Natural Science Foundation of China (Grant 41330964) and the Taishan Scholar Program of Shandong Province, China (Grant ts201511077).

ACKNOWLEDGMENTS

We are grateful to the editors and reviewers for their constructive comments on our manuscript.

REFERENCES

Aitken, M. J. (1990). *Science-based Dating in Archaeology*. London: Longman Archaeology Series.

Alexander, C. R., DeMaster, D. J., and Nittrouer, C. A. (1991). Sediment Accumulation in a Modern Epicontinental-Shelf Setting: The Yellow Sea. *Mar. Geology.* 98, 51–72. doi:10.1016/0025-3227(91)90035-3

Allen, M. B., Macdonald, D. I. M., Xun, Z., Vincent, S. J., and Brouet-Menzies, C. (1997). Early Cenozoic Two-Phase Extension and Late Cenozoic thermal Subsidence and Inversion of the Bohai Basin, Northern China. *Mar. Pet. Geology.* 14, 951–972. doi:10.1016/s0264-8172(97)00027-5

Anbuselvan, N., and Senthil Nathan, D. (2018). Benthic Foraminiferal Distribution and Biofacies in the Shelf Part of the Bay of Bengal, East Coast of India. *Mar. Biodiv.* 49, 691–706. doi:10.1007/s12526-018-0845-1

Antonioli, F., Bard, E., Potter, E.-K., Silenzi, S., and Improta, S. (2004). 215-ka History of Sea-Level Oscillations From marine and continental Layers in Argentarola Cave Speleothems (Italy). *Glob. Planet. Change* 43, 57–78. doi:10.1016/j.gloplacha.2004.02.004

Buylaert, J. P., Vandenberghe, D., Murray, A. S., Huot, S., De Corte, F., and Van den Haute, P. (2007). Luminescence Dating of Old (>70ka) Chinese Loess: A

Comparison of Single-Aliquot OSL and IRSL Techniques. *Quat. Geochronol.* 2, 9–14. doi:10.1016/j.quageo.2006.05.028

Chappell, J., Omura, A., Esat, T., McCulloch, M., Pandolfi, J., Ota, Y., et al. (1996). Reconciliaion of Late Quaternary Sea Levels Derived from Coral Terraces at the Huon Peninsula with Deep Sea Oxygen Isotope Records. *Earth Planet. Sci. Lett.* 141, 227–236. doi:10.1016/0012-821x(96)00062-3

Chen, Y. S., Wang, H., Pei, Y. D., Tian, L. Z., Li, J. F., and Shang, Z. W. (2012). Division and its Geological Significance of the Late Quaternary marine Sedimentary Beds in the West Coast of Bohai Bay, China. *J. Jilin Univ. (Earth Sci. Edition).* 42, 747–759. doi:10.3969/j.issn.1671-5888.2012.03.018

Columbu, A., Spötl, C., De Waele, J., Yu, T.-L., Shen, C.-C., and Gázquez, F. (2019). A Long Record of MIS 7 and MIS 5 Climate and Environment from a Western Mediterranean Speleothem (SW Sardinia, Italy). *Quat. Sci. Rev.* 220, 230–243. doi:10.1016/j.quascirev.2019.07.023

Dai, L., Li, S., Yu, J., Wang, J., Peng, B., Wu, B., et al. (2021). Palynological Evidence Indicates the Paleoclimate Evolution in Southeast China since Late Marine Isotope Stage 5. *Quat. Sci. Rev.* 266, 106964. doi:10.1016/j.quascirev.2021.106964

De Rijk, S., Troelstra, S. R., and Rohling, E. J. (1999). Benthic Foraminiferal Distribution in the Mediterranean Sea. *J. Foraminiferal Res.* 29, 93–103. doi:10.2113/gsjfr.29.2.93

Duller, G. A. T. (2003). Distinguishing Quartz and Feldspar in Single Grain Luminescence Measurements. *Radiat. Measurements.* 37, 161–165. doi:10.1016/s1350-4487(02)00170-1

Fagherazzi, S., Howard, A. D., Niedoroda, A. W., and Wiberg, P. L. (2008). Controls on the Degree of Fluvial Incision of continental Shelves. *Comput. Geosciences.* 34, 1381–1393. doi:10.1016/j.cageo.2008.02.004

Folk, R. L., and Ward, W. C. (1957). Brazos River Bar: a Study in the Significance of Grain Size Parameters. *J. Sediment. Petrology.* 31, 514–519.

Frontalini, F., and Coccioni, R. (2008). Benthic Foraminifera for Heavy Metal Pollution Monitoring: A Case Study from the central Adriatic Sea Coast of Italy. *Estuarine, Coastal Shelf Sci.* 76, 404–417. doi:10.1016/j.ecss.2007.07.024

Fu, S. Q., Zong, Y. Q., Xiong, H. X., Zhao, X. W., Zheng, Y. W., Wu, Y., et al. (2020). New Evidence for Sea Level Changes during the Marine Isotope Stage 5 in the Pearl River Delta. *Quat. Sci.* 40, 1095–1104. (in Chinese with English abstract). doi:10.11928/j.issn.1001-7410.2020.05.01

Gao, L., Long, H., Tamura, T., Hou, Y., and Shen, J. (2021). A ~130 Ka Terrestrial-marine Interaction Sedimentary History of the Northern Jiangsu Coastal plain in China. *Mar. Geology.* 435, 106455. doi:10.1016/j.margeo.2021.106455

Gao, L., Long, H., Zhang, P., Tamura, T., Feng, W., and Mei, Q. (2019). The Sedimentary Evolution of Yangtze River delta since MIS3: A New Chronology Evidence Revealed by OSL Dating. *Quat. Geochronol.* 49, 153–158. doi:10.1016/j.quageo.2018.03.010

Guo, X. W., Shi, X. B., Qiu, X. L., Wu, Z. P., Yang, X. Q., and Xiao, S. B. (2007). Cenozoic Subsidence in Bohai Bay Basin: Characteristics and Dynamic Mechanism. *Geotectonica Et Metallogenia.* 31, 273–280. (in Chinese with English abstract).

Hanebuth, T. J. J., Saito, Y., Tanabe, S., Vu, Q. L., and Ngo, Q. T. (2006). Sea Levels During Late Marine Isotope Stage 3 (Or Older?) Reported From the Red River Delta (Northern Vietnam) and Adjacent Regions. *Quat. Int.* 145-146 (146), 119–134. doi:10.1016/j.quaint.2005.07.008

Hayward, B. W., and Hollis, C. J. (1994). Brackish Foraminifera in New Zealand: A Taxonomic and Ecologic Review. *Micropaleontology.* 40, 185–222. doi:10.2307/1485816

Hinkel, J., Lincke, D., Vafeidis, A. T., Perrette, M., Nicholls, R. J., Tol, R. S. J., et al. (2014). Coastal Flood Damage and Adaptation Costs under 21st century Sea-Level Rise. *Proc. Natl. Acad. Sci. U.S.A.* 111, 3292–3297. doi:10.1073/pnas.1222469111

Huntley, D. J., and Baril, M. R. (1997). The K Content of the K-Feldspar Being Measured in Optical Dating or Thermoluminesence Dating. *Ancient TL.* 15, 11–13.

Jacobs, Z. (2008). Luminescence Chronologies for Coastal and marine Sediments. *Boreas.* 37, 508–535. doi:10.1111/j.1502-3885.2008.00054.x

Lai, Z.-P., and Wintle, A. G. (2006). Locating the Boundary between the Pleistocene and the Holocene in Chinese Loess Using Luminescence. *The Holocene.* 16, 893–899. doi:10.1191/0959683606hol980rr

Lai, Z., and Brückner, H. (2008). Effects of Feldspar Contamination on Equivalent Dose and the Shape of Growth Curve for OSL of Silt-Sized Quartz Extracted from Chinese Loess. *Geochronometria.* 30, 49–53. doi:10.2478/v10003-008-0010-0

Lai, Z. (2010). Chronology and the Upper Dating Limit for Loess Samples from Luochuan Section in the Chinese Loess Plateau Using Quartz OSL SAR Protocol. *J. Asian Earth Sci.* 37, 176–185. doi:10.1016/j.jseaes.2009.08.003

Lai, Z. P., and Ou, X. J. (2013). Basic Procedures of Optically Stimulated Luminescence (OSL) Dating. *Prog. Geogr.* 32, 683–693. doi:10.11820/dlkxjz.2013.05.001

Lai, Z. P., Zöller, L., Fuchs, M., and Brückner, H. (2008). Alpha Efficiency Determination for OSL of Quartz Extracted from Chinese Loess. *Radiat. Measurements.* 43, 767–770. doi:10.1016/j.radmeas.2008.01.022

Lai, Z. (2006). Testing the Use of an OSL Standardised Growth Curve (SGC) for Determination on Quartz from the Chinese Loess Plateau. *Radiat. Measurements.* 41, 9–16. doi:10.1016/j.radmeas.2005.06.031

Lambeck, K., and Chappell, J. (2001). Sea Level Change through the Last Glacial Cycle. *Science.* 292, 679–686. doi:10.1126/science.1059549

Li, B., Jacobs, Z., Roberts, R., and Li, S.-H. (2014). Review and Assessment of the Potential of post-IR IRSL Dating Methods to Circumvent the Problem of Anomalous Fading in Feldspar Luminescence. *Geochronometria.* 41, 178–201. doi:10.2478/s13386-013-0160-3

Li, B., Li, S.-H., Wintle, A. G., and Zhao, H. (2007). Isochron Measurements of Naturally Irradiated K-Feldspar Grains. *Radiat. Measurements.* 42, 1315–1327. doi:10.1016/j.radmeas.2007.09.008

Li, Y., Shang, Z., Tsukamoto, S., Tamura, T., Yi, L., Wang, H., et al. (2018). Quartz and K-Feldspar Luminescence Dating of Sedimentation in the North Bohai Coastal Area (NE China) since the Late Pleistocene. *J. Asian Earth Sci.* 152, 103–115. doi:10.1016/j.jseaes.2017.10.036

Li, Y., Tsukamoto, S., Shang, Z., Tamura, T., Wang, H., and Frechen, M. (2019). Constraining the Transgression History in the Bohai Coast China since the Middle Pleistocene by Luminescence Dating. *Mar. Geology.* 416, 105980. doi:10.1016/j.margeo.2019.105980

Lisá, L., Neruda, P., Nerudová, Z., and nejman, L. (2018). Podhradem Interstadial; A Critical Review of the Middle and Late MIS 3 (Denekamp, Hengelo) in Moravia, Czech Republic. *Quat. Sci. Rev.* 182, 191–201. doi:10.1016/j.quascirev.2017.12.024

Lisiecki, L. E., and Raymo, M. E. (2005). A PlioceneePleistocene Stack of 57 Globally Distributed Benthic δ18O Records. *Paleoceanography* 20, PA1003. doi:10.1029/2004pa001071

Liu, J., Saito, Y., Kong, X., Wang, H., Wen, C., Yang, Z., et al. (2010). Delta Development and Channel Incision during Marine Isotope Stages 3 and 2 in the Western South Yellow Sea. *Mar. Geology.* 278, 54–76. doi:10.1016/j.margeo.2010.09.003

Liu, J., Saito, Y., Wang, H., Yang, Z., and Nakashima, R. (2007). Sedimentary Evolution of the Holocene Subaqueous Clinoform off the Shandong Peninsula in the Yellow Sea. *Mar. Geology.* 236, 165–187. doi:10.1016/j.margeo.2006.10.031

Liu, J., Saito, Y., Wang, H., Zhou, L., and Yang, Z. (2009). Stratigraphic Development during the Late Pleistocene and Holocene Offshore of the Yellow River delta, Bohai Sea. *J. Asian Earth Sci.* 36, 318–331. doi:10.1016/j.jseaes.2009.06.007

Liu, J., Shi, X., Liu, Q., Ge, S., Liu, Y., Yao, Z., et al. (2014). Magnetostratigraphy of a Greigite-Bearing Core from the South Yellow Sea: Implications for Remagnetization and Sedimentation. *J. Geophys. Res. Solid Earth.* 119, 7425–7441. doi:10.1002/2014jb011206

Liu, J., Wang, H., Wang, F., Qiu, J., Saito, Y., Lu, J., et al. (2016). Sedimentary Evolution during the Last ~ 1.9 Ma Near the Western Margin of the Modern Bohai Sea. *Palaeogeogr. Palaeoclimatol. Palaeoecol.* 451, 84–96. doi:10.1016/j.palaeo.2016.03.012

Liu, J., Zhang, X., Mei, X., Zhao, Q., Guo, X., Zhao, W., et al. (2018). The Sedimentary Succession of the Last ~ 3.50 Myr in the Western South Yellow Sea: Paleoenvironmental and Tectonic Implications. *Mar. Geology.* 399, 47–65. doi:10.1016/j.margeo.2017.11.005

Long, H., Tsukamoto, S., Buylaert, J.-P., Murray, A. S., Jain, M., and Frechen, M. (2019). Late Quaternary OSL Chronologies from the Qinghai Lake (NE Tibetan Plateau): Inter-comparison of Quartz and K-Feldspar Ages to Assess the Pre-

depositional Bleaching. *Quat. Geochronol.* 49, 159–164. doi:10.1016/j.quageo.2018.05.003

Lowick, S. E., and Preusser, F. (2011). Investigating Age Underestimation in the High Dose Region of Optically Stimulated Luminescence Using fine Grain Quartz. *Quat. Geochronol.* 6, 33–41. doi:10.1016/j.quageo.2010.08.001

Manaa, A. A., Jones, B. G., McGregor, H. V., Zhao, J.-x., and Price, D. M. (2016). Dating Quaternary Raised Coral Terraces along the Saudi Arabian Red Sea Coast. *Mar. Geology.* 374, 59–72. doi:10.1016/j.margeo.2016.02.002

Miller, G. H., and Andrews, J. T. (2019). Hudson Bay Was Not Deglaciated during MIS-3. *Quat. Sci. Rev.* 225, 105944. doi:10.1016/j.quascirev.2019.105944

Milliman, J. D., Qin, Y. S., Ren, M. E., and Saito, Y. (1987). Man's Influence on the Erosion and Transport of Sediment by Asian Rivers: The Yellow River (Huanghe) Example. *J. Geol.* 95, 751–762. doi:10.2307/30063822

Murray, A., Arnold, L. J., Buylaert, J.-P., Guerin, G., Qin, J. T., Singhvi, A. K., et al. (2021). Optically Stimulated Luminescence Dating Using Quartz. *Nat. Rev. Methods Primers.* 1, 1–31. doi:10.1038/s43586-021-00068-5

Murray, A. S., Svendsen, J. I., Mangerud, J., and Astakhov, V. I. (2007). Testing the Accuracy of Quartz OSL Dating Using a Known-Age Eemian Site on the River Sula, Northern Russia. *Quat. Geochronol.* 2, 102–109. doi:10.1016/j.quageo.2006.04.004

Murray, A. S., and Wintle, A. G. (2000). Luminescence Dating of Quartz Using an Improved Single-Aliquot Regenerative-Dose Protocol. *Radiat. Measurements.* 32, 57–73. doi:10.1016/s1350-4487(99)00253-x

Neudorf, C. M., Lian, O. B., Walker, I. J., Shugar, D. H., Eamer, J. B. R., and Griffin, L. C. M. (2015). Toward a Luminescence Chronology for Coastal Dune and beach Deposits on Calvert Island, British Columbia central coast, Canada. *Quat. Geochronol.* 30, 275–281. doi:10.1016/j.quageo.2014.12.004

Nian, X., Zhang, W., Wang, Z., Sun, Q., and Chen, Z. (2021). Inter-comparison of Optically Stimulated Luminescence (OSL) Ages between Different Fractions of Holocene Deposits from the Yangtze delta and its Environmental Implications. *Mar. Geology.* 432, 106401. doi:10.1016/j.margeo.2020.106401

Olley, J., Caitcheon, G., and Murray, A. (1998). The Distribution of Apparent Dose as Determined by Optically Stimulated Luminescence in Small Aliquots of Fluvial quartzImplications for Dating Young Sediments. *Quat. Sci. Rev.* 17, 1033–1040. doi:10.1016/s0277-3791(97)00090-5

Pawley, S. M., Toms, P., Armitage, S. J., and Rose, J. (2010). Quartz Luminescence Dating of Anglian Stage (MIS 12) Fluvial Sediments: Comparison of SAR Age Estimates to the Terrace Chronology of the Middle Thames Valley, UK. *Quat. Geochronol.* 5, 569–582. doi:10.1016/j.quageo.2009.09.013

Pico, T., Mitrovica, J. X., Ferrier, K. L., and Braun, J. (2016). Global Ice Volume during MIS 3 Inferred from a Sea-Level Analysis of Sedimentary Core Records in the Yellow River Delta. *Quat. Sci. Rev.* 152, 72–79. doi:10.1016/j.quascirev.2016.09.012

Pigati, J. S., Quade, J., Wilson, J., Jull, A. J. T., and Lifton, N. A. (2007). Development of Low-Background Vacuum Extraction and Graphitization Systems for 14c Dating of Old (40–60 Ka) Samples. *Quat. Int.* 166, 4–14. doi:10.1016/j.quaint.2006.12.006

Qian, S. L., Liu, J., Wang, P. P., Zhang, X., Wang, F. F., and An, Y. H. (2021). The Sedimentary Succession of Core YRD-1401 in the Modern Yellow River Delta since MIS 5 and its Paleoenvironmental Significance. *Quat. Sci.* 41, 1317–1331. (in Chinese with English abstract). doi:10.11928/j.issn.1001-7410.2021.05.08

Qiao, S., Shi, X., Saito, Y., Li, X., Yu, Y., Bai, Y., et al. (2011). Sedimentary Records of Natural and Artificial Huanghe (Yellow River) Channel Shifts during the Holocene in the Southern Bohai Sea. *Continental Shelf Res.* 31, 1336–1342. doi:10.1016/j.csr.2011.05.007

Qin, Y. C., Mei, X., Jiang, X., Luan, X., Zhou, L., and Zhu, X. (2021). Sediment Provenance and Tidal Current-Driven Recycling of Yellow River Detritus in the Bohai Sea, China. *Mar. Geology.* 436, 106473. doi:10.1016/j.margeo.2021.106473

Qin, Y. C., Sun, R. T., Wang, H., Tian, Z. X., Xu, Y., and Wen, Z. H. (2020). Transgressive Succession Offshore Rizhao in Western South Yellow Sea and Paleo-Environmental Implications. *Acta Sedimentologica Sinica.* 38, 790–809. doi:10.14027/j.issn.1000-0550.2019.063

Qin, Y. S., and Zhao, S. L. (1985). The Sedimentary Model and Quaternary Transgressions in the continental Shelf of China. *Quat. Sci.* 6, 27–34.

Qin, Y. S., Zhao, Y. Y., Chen, L. R., and Zhao, S. L. (1990). *Geology of Bohai Sea*. Beijing: China Ocean Press.

Reimann, T., Naumann, M., Tsukamoto, S., and Frechen, M. (2010). Luminescence Dating of Coastal Sediments from the Baltic Sea Coastal Barrier-Spit Darss-Zingst, NE Germany. *Geomorphology.* 122, 264–273. doi:10.1016/j.geomorph.2010.03.001

Reineck, H. E., and Singh, I. B. (1980). *Depositional Sedimentary Environments*. Second ed. Berlin: Springer-Verlag.

Roberts, H. M., and Duller, G. A. T. (2004). Standardised Growth Curves for Optical Dating of Sediment Using Multiple-Grain Aliquots. *Radiat. Measurements.* 38, 241–252. doi:10.1016/j.radmeas.2003.10.001

Romano, E., Bergamin, L., Pierfranceschi, G., Provenzani, C., and Marassich, A. (2018). The Distribution of Benthic Foraminifera in Bel Torrente Submarine Cave (Sardinia, Italy) and Their Environmental Significance. *Mar. Environ. Res.* 133, 114–127. doi:10.1016/j.marenvres.2017.12.014

Ronchi, L., Fontana, A., Correggiari, A., and Asioli, A. (2018). Late Quaternary Incised and Infilled Landforms in the Shelf of the Northern Adriatic Sea (Italy). *Mar. Geology.* 405, 47–67. doi:10.1016/j.margeo.2018.08.004

Rowe, M. P., Wainer, K. A. I., Bristow, C. S., and Thomas, A. L. (2014). Anomalous MIS 7 Sea Level Recorded on Bermuda. *Quat. Sci. Rev.* 90, 47–59. doi:10.1016/j.quascirev.2014.02.012

Saito, Y., Wei, H., Zhou, Y., Nishimura, A., Sato, Y., and Yokota, S. (2000). Delta Progradation and Chenier Formation in the Huanghe (Yellow River) delta, China. *J. Asian Earth Sci.* 18, 469–497. doi:10.1016/s1367-9120(99)00080-2

Shackleton, N. J. (1987). Oxygen Isotopes, Ice Volume, and Sea Level. *Quat. Sci. Rev.* 6, 183–190. doi:10.1016/0277-3791(87)90003-5

Shang, S., Fan, D., Yin, P., Burr, G., Zhang, M., and Wang, Q. (2018). Late Quaternary Environmental Change in Oujiang delta along the Northeastern Zhe-Min Uplift Zone (Southeast China). *Palaeogeogr. Palaeoclimatol. Palaeoecol.* 492, 64–80. doi:10.1016/j.palaeo.2017.12.012

Shepard, F. P. (1954). Nomenclature Based on sand–silt–clay Ratios. *J. Sediment. Petrology.* 24, 151–158. doi:10.1306/d426971a-2b26-11d7-8648000102c1865d

Shi, X., Yao, Z., Liu, Q., Larrasoaña, J. C., Bai, Y., Liu, Y., et al. (2016). Sedimentary Architecture of the Bohai Sea China over the Last 1 Ma and Implications for Sea-Level Changes. *Earth Planet. Sci. Lett.* 451, 10–21. doi:10.1016/j.epsl.2016.07.002

Singarayer, J. S., and Bailey, R. M. (2003). Further Investigations of the Quartz Optically Stimulated Luminescence Components Using Linear Modulation. *Radiat. Measurements.* 37, 451–458. doi:10.1016/s1350-4487(03)00062-3

Southon, J., Kashgarian, M., Fontugne, M., Metivier, B., and W-S Yim, W. (2002). Marine Reservoir Corrections for the Indian Ocean and Southeast Asia. *Radiocarbon.* 44, 167–180. doi:10.1017/s0033822200064778

Straub, K. M., Duller, R. A., Foreman, B. Z., and Hajek, E. A. (2020). Buffered, Incomplete, and Shredded: The Challenges of Reading an Imperfect Stratigraphic Record. *J. Geophys. Res. Earth Surf.* 125, e2019JF005079. doi:10.1029/2019jf005079

Stuiver, M., and Reimer, P. (1986). *Calib Radiocarbon Calibration Program*.

Timar, A., Vandenberghe, D., Panaiotu, E. C., Panaiotu, C. G., Necula, C., Cosma, C., et al. (2010). Optical Dating of Romanian Loess Using fine-grained Quartz. *Quat. Geochronol.* 5, 143–148. doi:10.1016/j.quageo.2009.03.003

Wang, Z. H., Jones, B. G., Chen, T., Zhao, B. C., and Zhan, Q. (2013). A raised OIS 3 sea level recorded in coastal sediments, southern Changjiang delta plain, China. *Quaternary Res* 79, 424–438. doi:10.1016/j.yqres.2013.03.002

Wang, F., Chen, Y. S., Li, J. F., Wang, H., Fang, J., Shang, Z. W., et al. (2014). The Age of the Second marine Layer in Coastal lowland of Bohai Bay Revealed by AMS ^{14}C Dating Method. *Geol. Bull. China* 33, 1591–1595. (in Chinese with English abstract). doi:10.3969/j.issn.1671-2552.2014.10.016

Wang, H., Yang, Z., Saito, Y., Liu, J. P., Sun, X., and Wang, Y. (2007). Stepwise Decreases of the Huanghe (Yellow River) Sediment Load (1950–2005): Impacts of Climate Change and Human Activities. *Glob. Planet. Change.* 57, 331–354. doi:10.1016/j.gloplacha.2007.01.003

Wang, P. X., Min, Q. B., Bian, Y. H., and Chen, X. R. (1981). Strata of Quaternary Transgressions in east China: a Preliminary Study. *Acta Geokiguca Sinica.* 1, 1–13. (in Chinese with English abstract). CNKI:SUN:DZXE.0.1981-01-000

Wang, Q., and Tian, G. Q. (1999). The Neotectonic Setting of Late Quaternary Transgressions on the Eastern Coastal plain of China. *J. Geomechanics* 5, 41–48. (in Chinese with English abstract). doi:10.3969/j.issn.1006-6616.1999.04.005

Wang, Z. B., Zhang, J. Y., Mei, X., Chen, X. H., Zhao, L., Zhang, Y., et al. (2020). The Stratigraphy and Depositional Environments of China's Sea Shelves since MIS5

74-128 Ka. *Geology. China.* 47, 1370–1394. (in Chinese with English abstract). doi:10.12029/gc20200506

Wang, Z. H., Zhao, B. C., Chen, J., and Li, X. (2008). Chronostratigraphy and Two Transgressions during the Late Quaternary in Changjiang delta Area. *J. Paleogeography.* 10, 99–110. CNKI:SUN:GDLX.0.2008-01-017

Wang, Z., Zheng, H., Mei, X., Meng, X., Xu, T., Wang, Z., et al. (2021). Sedimentary Environment Evolution and Provenance Analysis of Northwestern Liaodong Bay from the Middle Pleistocene. *Quat. Int.* 589, 55–67. doi:10.1016/j.quaint.2020.11.041

Wintle, A. G., and Murray, A. S. (2006). A Review of Quartz Optically Stimulated Luminescence Characteristics and Their Relevance in Single-Aliquot Regeneration Dating Protocols. *Radiat. Measurements.* 41, 369–391. doi:10.1016/j.radmeas.2005.11.001

Xu, Q. M., Yuan, G. B., Zhang, J. Q., and Qin, Y. F. (2011). Stratigraphic Division of the Late Quaternary Strata along the Coast of Bohai Bay and its Geology Significance. *Acta Geologica Sinica* 85, 1352–1367. 11-1951/P.20110804.1239.004

Xu, Q., Yang, J., Hu, Y., Yuan, G., and Deng, C. (2018). Magnetostratigraphy of Two Deep Boreholes in Southwestern Bohai Bay: Tectonic Implications and Constraints on the Ages of Volcanic Layers. *Quat. Geochronol.* 43, 102–114. doi:10.1016/j.quageo.2017.08.006

Xue, C. (1993). Historical Changes in the Yellow River delta, China. *Mar. Geology.* 113, 321–330. doi:10.1016/0025-3227(93)90025-q

Yan, Y. G., Wang, H., Li, F. L., Li, J. F., Zhao, C. R., and Lin, F. (2006). Sedimentary environment and sea-level fluctuations revealed by Borehole BQ1 on the west coast of the Bohai Sea, China. *Geological Bulletin of China* 25, 357–382. (Earth Sci. Edition) CNKI:SUN:ZQYD.0.2006-03-006

Yang, Z. G., Lin, H. M., Wang, S. J., and Li, S. Q. (1998). A Study of the Ancient Cold Water Mass Sediments in South Yellow Sea during Last Interglacial. *Mar. Geology. Quat. Geology.* 18, 47–58. doi:10.16562/j.cnki.0256-1492.1998.01.007

Yao, J., Yu, H. J., Xu, X. Y., Yi, L., and Su, Q. (2010). Deposition Characteristics in Brine Aquifers and Brine Formation in Laizhou Bay Area. *Adv. Mar. Sci.* 28, 473–477. doi:10.3969/j.issn.1671-6647.2010.04.007

Yi, L., Deng, C., Tian, L., Xu, X., Jiang, X., Qiang, X., et al. (2016). Plio-Pleistocene Evolution of Bohai Basin (East Asia): Demise of Bohai Paleolake and Transition to marine Environment. *Sci. Rep.* 6, 29403–29409. doi:10.1038/srep29403

Yi, L., Yu, H.-J., Ortiz, J. D., Xu, X.-Y., Chen, S.-L., Ge, J.-Y., et al. (2012). Late Quaternary Linkage of Sedimentary Records to Three Astronomical Rhythms and the Asian Monsoon, Inferred from a Coastal Borehole in the South Bohai Sea, China. *Palaeogeogr. Palaeoclimatol. Palaeoecol.* 329-330, 101–117. doi:10.1016/j.palaeo.2012.02.020

Yim, W. W.-S., Ivanovich, M., and Yu, K.-F. (1990). Young Age Bias of Radiocarbon Dates in Pre-Holocene marine Deposits of Hong Kong and Implications for Pleistocene Stratigraphy. *Geo-Marine Lett.* 10, 165–172. doi:10.1007/bf02085932

Zhang, X., Liu, J., Wang, F. F., Qiu, J. D., and Wang, S. (2016). Study of Optically Stimulated Luminescence (OSL) Chronology and Sedimentary Environments of the Yellow River Delta Area with Core YRD-1402. *Mar. Geology. Quat. Geology.* 36, 11–22. (in Chinese with English abstract). doi:10.16562/j.cnki.0256-1492.2016.03.002

Zhao, B., Wang, Z., Chen, J., and Chen, Z. (2008). Marine Sediment Records and Relative Sea Level Change during Late Pleistocene in the Changjiang delta Area and Adjacent Continental Shelf. *Quat. Int.* 186, 164–172. doi:10.1016/j.quaint.2007.08.006

Zhao, S. L., Yang, G. F., Cang, S. X., Zhang, H. C., Huang, Q. F., Xia, D. X., et al. (1978). On the marine Stratigraphy and Coastline of the Western Coast of the Gulf of Bohai. *Oceanologia et Limnologia Sinica* 9, 15–25. (in Chinese with English abstract).

Zhou, L., Liu, J., Saito, Y., Liu, J. P., Li, G., Liu, Q., et al. (2014). Fluvial System Development and Subsequent marine Transgression in Yellow River (Huanghe) delta and its Adjacent Sea Regions during Last Glacial Maximum to Early Holocene. *Continental Shelf Res.* 90, 117–132. doi:10.1016/j.csr.2014.06.012

Conflict of Interest: The authors declare that the research was conducted in the absence of any commercial or financial relationships that could be construed as a potential conflict of interest.

Publisher's Note: All claims expressed in this article are solely those of the authors and do not necessarily represent those of their affiliated organizations, or those of the publisher, the editors, and the reviewers. Any product that may be evaluated in this article, or claim that may be made by its manufacturer, is not guaranteed or endorsed by the publisher.